

Spontaneous synchronization driven by energy transport in interconnected networks

Vincenzo Nicosia,^{1,*} Per Sebastian Skardal,^{2,*} Vito Latora,¹ and Alex Arenas²

¹*School of Mathematical Sciences, Queen Mary University of London, Mile End Road, E1 4NS, London (UK)*

²*Departament d'Enginyeria Informàtica i Matemàtiques, Universitat Rovira i Virgili, 43007 Tarragona, Spain*

The existence of intertwined dynamical processes in interconnected networks is a distinctive aspect of complex systems. For example, cerebral circulation delivers oxygenated blood to the brain through blood vessels, and in turn the neural system in the brain is responsible, through neural network connections, for mediating changes in cerebral blood flow. To understand the effects of the coupling between different processes we study the case of two interconnected networks, one accounting for energy transport and the other for a synchronization dynamics. We observe the emergence of switch-like spontaneous synchronization, similar to that seen in the transition between resting-state and cognitive activity in the human brain, for a wide range of control parameters and for different network topologies. We suggest that similarly interconnected dynamical processes could be responsible for spontaneous synchronization transitions observed in natural systems.

PACS numbers: 89.75.Hc, 05.45.Xt, 05.40.Fb

Complex systems very often consists of large networks of interacting units [1, 2] and are characterised by a variety of intertwined dynamics [3]. To date the topic of interacting dynamical processes on interconnected networks remains a largely unexplored area of scientific research, apart from a few pioneering studies [4, 5]. This is mostly due to the great complexity inherent in such systems, which usually result from the co-evolution of diverse dynamical processes, taking place on different interaction networks and interconnected by relationships of different nature. A wonderful example of this complexity is the human brain, whose activity is the combination of several dynamics, including blood flow, oxygen exchange, chemical and electrical interactions among neurons, and remote synchronization of distant regions [6–8]. Here we present a natural formulation for this kind of systems based on a multiplex representation [9, 10] inspired to the human brain. In general, a multiplex consists of a set of N nodes and L network layers. Each layer has its own distinct network topology, with the links of a layer representing a different kind of interaction among nodes [11–13]. Thus, a given node is described by a distinct connectivity pattern on each layer and by a state vector whose components are the state variables associated to its dynamics at each level. In particular, we consider the case of a multiplex with two layers, representing respectively an energy transport network and a synchronization network, as shown in Fig. 1. The adjacency matrices encoding the topology of the transport and synchronization layers are denoted $E = \{e_{ij}\}$ and $A = \{a_{ij}\}$, respectively, and we denote by $q_i = \sum_{j=1}^N e_{ij}$ and $k_i = \sum_{j=1}^N a_{ij}$ the degrees of node i at the two layers. Importantly, the two dynamic processes occurring at the two layers, transportation and synchronization, are non-trivially coupled in both directions.

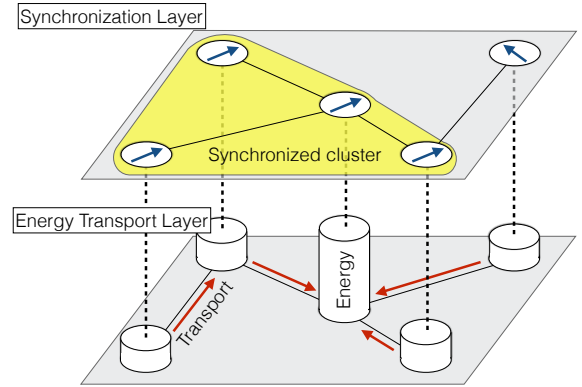


FIG. 1. Multiplex networks. Illustration of a multiplex with two layers accounting, respectively, for the synchronization of coupled Kuramoto oscillators and for the transport of random walkers (energy packets). Note that there is a one-to-one correspondence between the nodes in each layer, while each layer has different connectivity properties, so that a node i has degree q_i at the first layer and k_i at the second. The state of a node i at a given time t is characterized by the phase $\theta_i(t)$ of the oscillator at the synchronization layer and by the probability p_i^t of finding a walker at node i on the transport network. The two processes, transport and synchronization, are coupled in such a way that the synchronization dynamics at a node depends on its availability of energy (namely the oscillator frequency of a node in the synchronization layer is proportional to the available energy in the transport layer) and, at the same time, the motion of energy in the transport layer is biased according to the degree of the node in the synchronization network.

Transportation layer. Energy transportation is modeled as a biased random walk process [14], in which a continuum of walkers, each interpreted as a “packet” of energy, diffuse throughout the network. Namely, we assume that the probability π_{ji} for a walker to move from

* These authors have equally contributed to this work

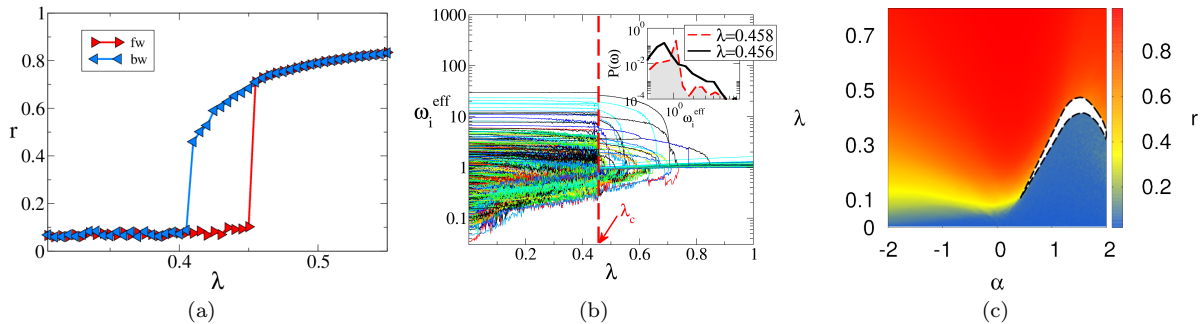


FIG. 2. **Intertwined dynamics foster spontaneous synchronization.** (a) Forward (red) and backward (blue) synchronization order parameter r as a function of the coupling strength λ for a multiplex system in which Kuramoto-like synchronization of oscillators on one layer is intertwined with energy transport modeled as an α -biased random walk ($\alpha = 1.4$) on the other layer. The transition to synchronization is abrupt and exhibits a hysteresis loop. (b) The spontaneous synchronization transition corresponds, at a microscopic level, to the sudden alignment of the effective frequencies ω_i^{eff} of an extensive fraction of the nodes, due to an infinitesimal increase of the coupling strength above the critical value $\lambda_c \simeq 0.457$, indicated by the dashed red line. The inset shows the distribution of ω_i^{eff} before (solid black line) and after the transition (dashed red line). (c) Phase diagram showing r as a function of α and λ . The white area bordered by dashed lines indicates the bistable region. Synchronization is explosive for $0.6 < \alpha < 2.0$. As α increases, the critical value of λ at which the system switches to the synchronized state increases up until $\alpha \simeq 1.5$, and then decreases again.

node i to node j is equal to:

$$\pi_{ji} = \frac{e_{ij} k_j^\alpha}{\sum_l e_{il} k_l^\alpha}, \quad (1)$$

where α is a control parameter to tune the bias. In particular, for $\alpha > 0$ ($\alpha < 0$) movement is biased towards nodes with large (small) degree in the *synchronization layer*, whereas $\alpha = 0$ corresponds to the unbiased case in which all nodes in the transportation network are selected with uniform probability. The probability p_i^t of finding a given walker on node i at time t evolves according to:

$$p_j^{t+1} = \sum_{i=1}^N \pi_{ji} p_i^t. \quad (2)$$

Synchronization layer. Synchronization is modeled by an ensemble of N Kuramoto oscillators θ_i on the synchronization layer [15, 16], where oscillators evolve according to

$$\dot{\theta}_i = \omega_i + \lambda \sum_{j=1}^N a_{ij} \sin(\theta_j - \theta_i), \quad (3)$$

where ω_i is the natural frequency of the oscillator and λ is the coupling strength. To make the dynamics of Eq. (3) depend on the dynamics and structure of the *transport layer*, we assume that the frequency ω_i is proportional to p_i , the amount of energy at node i . Without any loss of generality we set $\omega_i = N p_i$, so that the average natural frequency is equal to one. The degree of synchronization of the system is measured by the magnitude r of the complex order parameter $r e^{i\psi} = N^{-1} \sum_{j=1}^N e^{i\theta_j}$. In

particular, the cases $r \approx 0$ and $r \approx 1$ correspond, respectively, to incoherent and synchronized states.

The key element in our model is that each node of the system participates to both layers, so that synchronization and energy transport are naturally intertwined. This choice is inspired by studies that have confirmed the existence of relatively strong correlations between the electrical activity of a brain area and the hematic inflow in the same area, which is responsible for the transport of energy to the neurons in the form of oxygen molecules [17–19]. In our model the synchronization dynamics of a given node i depends on the availability of energy at i , and vice-versa the abundance of energy packets on i depends on the participation of i in the synchronization layer.

We now show that the interplay of the two processes naturally produces spontaneous synchronization, even when the transport and synchronization layer topologies are uncorrelated. We illustrate this by considering a scale-free (SF) network as the synchronization layer, and an Erdős-Rényi (ER) random graph as the transport layer [20] with $N = 1000$ nodes each. The SF network is built using the configuration model [21] on a degree sequence drawn from a power-law distribution $P(k) \propto k^{-\gamma}$ with $\gamma = 2.8$ and enforced minimum degree $k_0 = 3$. For the ER network we used a link probability $p = 0.01$. The results are summarized in Fig. 2, for different values of the bias parameter α .

The main finding is the appearance of spontaneous synchronization, i.e., a first-order phase transition which produces the spontaneous synchronization of the oscillators on the synchronization layer. Fig. 2 (a) confirms that the transition to synchronization is sharp and is charac-

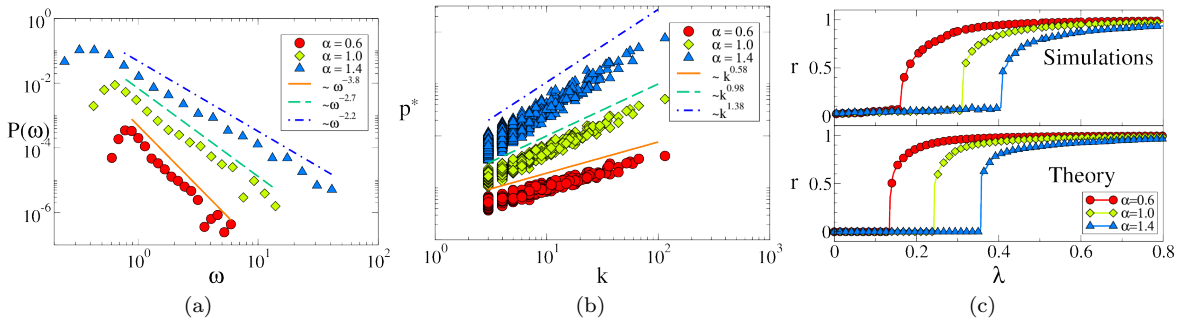


FIG. 3. **Agreement between theory and simulations.** (a) The value of the motion bias substantially affects the distribution of the oscillators’ natural frequencies, so that smaller values of α correspond to more homogeneous distributions of ω_i , and vice-versa. In particular, when the transport layer is a random graph and the synchronization layer is a scale-free graph $P(k) \sim k^{-\gamma}$, we have $P(\omega) \sim \omega^{-\frac{\gamma}{\alpha}}$. (b) There is a clear correlation between the degree of a node on the synchronization layer and the natural frequency of the corresponding oscillator. In the simulations we observe $p_i^* \propto k_i^\alpha$, as expected. (c) The theory is also able to predict quite well the explosive transition to synchronization observed in the simulations. In particular, the value of r obtained by solving Eq. (4) for different values of λ (bottom panel) closely correspond to the backward synchronization diagrams of the simulated system (top panel). The plots in panel (a) and (b) were vertically displaced to enhance readability.

terized by a hysteresis loop. As shown in Fig. 2 (b), where we report the average effective node frequency $\omega_i^{\text{eff}} = T^{-1} \int_t^{t+T} \dot{\theta}_i(t) dt$, $T \gg 1$ of each oscillator as a function of λ , at the critical value $\lambda_c \simeq 0.457$ the effective frequency of an extensive fraction of oscillators suddenly jumps to the same value $\bar{\omega} \simeq 1.0$, despite the huge variance in the values of ω_i^{eff} observed for $\lambda < \lambda_c$ (see inset). In Fig. 2 (c) we report the phase diagram of the system as a function of α and λ , where the bistable region is indicated in white. We note in particular that the explosive synchronization transition is quite robust and persists across a wide range of values of the bias parameter $0.6 < \alpha < 2.0$.

Spontaneous synchronization in the form of first-order explosive phase transitions has been found in a series of recent studies [22–24] where structural and dynamical correlations are artificially introduced in a single-layer network. Here, the appearance of an explosive synchronization transition is naturally due to the intertwined dynamics of energy transport and synchronization, and not to artificially imposed external constraints on the distribution of frequencies. Remarkably, qualitatively similar behavior is observed when the transport and synchronization layers have different topologies (see Appendix for details).

Despite the intrinsic complexity of the system, the steady-state dynamics of the model can be described analytically. It is in fact possible to find an analytical expression for the stationary distribution of energy packets on the transport layer p_i^* (see Appendix). Assuming no structural correlations between the two layers, p_i^* scales as $k_i^\alpha q_i$. Moreover, if the transport layer is an ER graph, for which $q_i \approx \langle q \rangle = p(N-1)$, we obtain $p_i^* \propto k_i^\alpha$. This scaling is accurately reproduced by the simulations, as shown in Fig. 3 (a) for different values of α . It is also worth noticing that the value of the motion bias actu-

ally modifies the distribution of the natural frequencies of the oscillators. In the particular case of a SF synchronization layer with $P(k) \sim k^{-\gamma}$ we have that, on average, $P(\omega) \sim \omega^{-\gamma/\alpha}$, as shown in Fig. 3 (b).

The synchronization dynamics can also be described analytically using a self-consistency analysis. Given a set of degree-frequency pairs $\{(k_i, \omega_i)\}_{i=1}^N$, the degree of synchronization r and the velocity Ω of the synchronized cluster at steady-state approximately satisfy

$$r = \frac{\langle k \rangle^{-1}}{N} \sum_{|\omega_j - \Omega| \leq \lambda r k_j} k_j \sqrt{1 - \left(\frac{\omega_j - \Omega}{\lambda r k_j} \right)^2}, \quad (4)$$

$$\Omega = \frac{\sum_{|\omega_j - \Omega| \leq \lambda r k_j} \omega_j}{\sum_{|\omega_j - \Omega| \leq \lambda r k_j}}, \quad (5)$$

A full derivation of Eqs. (4) and (5) is reported in the Appendix. As shown in Fig. 3 (c), the expression of r given by Eq. (4) reproduces quite well the transition to synchronization.

Experimental studies have confirmed that the electrical activity registered in a brain area is very often correlated with the dynamics of hematic flow in the same region [17–19], and that in some cases the hematic inflow of a brain region can be indeed triggered by neuronal activity [25, 26]. However, mainstream research in neuroimaging has mostly focused so far on understanding each of these processes separately, by looking either at electroencephalographic/magnetoencephalographic signals (EEG/MEG) or at hematic signals (fMRI) [8]. Intriguingly, the spontaneous synchronization observed in our interconnected networks model closely mirrors that displayed by the human brain [7], which continuously (and very quickly) switches between complex intellectual and motor tasks, and the so-called “resting-state activity”, which is the background activity of a brain when no particular con-

scious task is performed [27]. Recent results based on different neuroimaging techniques seem to suggest that resting-state is not just the idle interval between two consecutive mental tasks, but is instead a particular configuration which is flexible enough to allow, upon the receipt of an appropriate exogenous stimulus, the quick and massive reconfiguration of brain activity needed for the performance of any particular task [7, 28–30]. This flexibility requires the availability of efficient switch-like mechanisms, as those exhibited by our model, in which either a slight perturbation of the rule governing energy distribution or a small increase in the strength of interaction among neurons, can easily induce a sudden, massive synchronization.

In conclusion, we hypothesize that a more in-depth analysis of the relationship between hematic flow and neuronal activity might provide a more accurate description of brain activity as the result of different interconnected and co-evolving dynamics. At the same time, the modeling strategy proposed here might prove useful to understand the functioning principles of other systems consisting of different but interacting dynamical processes on interdependent networks which give rise to intriguing dynamics.

ACKNOWLEDGMENTS

V.N. and V.L. acknowledge support from the Project LASAGNE, Contract No.318132 (STREP), funded by the European Commission. P.S.S. acknowledges support from the James S. McDonnell Foundation.

Appendix A: Biased Random Walks

The classical Brownian walk on a graph can be easily extended to account for walkers to avoid (or prefer) to move towards nodes having certain structural properties, obtaining a *biased random walk* [14]. In its most general formulation, the motion rule of a discrete time biased random walk is described by the probability π_{ji} of moving from node i to node j and can be expressed as

$$\pi_{ji} = \frac{e_{ij} f_j}{c_i} \quad (\text{A1})$$

where e_{ij} are the entries of the adjacency matrix of the graph (i.e., $e_{ij} = 1$ if i and j are connected by an edge, and $e_{ij} = 0$ otherwise) and f_j is a function of any structural property of the destination node j . The term c_i is a constant that ensures $\sum_j \pi_{ji} = 1$, and thus $c_i = \sum_\ell e_{i\ell} f_\ell$. A typical choice for the bias function f is

$$f_j = x_j^\alpha \quad (\text{A2})$$

where x_j is a given structural property of node j (e.g. its nodal degree, eigenvector centrality, betweenness centrality, etc.) and α is a tunable parameter. In particular, for

$\alpha > 0$ then the walkers will preferentially move towards nodes with a large value of x_j , for $\alpha < 0$ the walkers will prefer to move towards nodes with small values of x_j , and for $\alpha = 0$ we recover the classical (unbiased) random walk. If we denote by p_i^t the fraction of random walkers found at time t at node i and by $\Pi = \{\pi_{ji}\}$ the column-stochastic transition matrix associated to the walk, the dynamical evolution of the process is governed by the discrete time recurrence equation:

$$\mathbf{p}^{t+1} = \Pi^T \mathbf{p}^t. \quad (\text{A3})$$

It is possible to show that if the underlying graph is primitive (i.e., if it consists of a single connected component and has at least one odd cycle), then independently of the initial distribution of walkers \mathbf{p}^0 and for any choice of the bias function f_j , the process converges to the stationary occupation probability given by

$$p_i^* = \frac{c_i f_i}{\sum_\ell c_\ell f_\ell}. \quad (\text{A4})$$

Notice that Eq. (A4) says that the stationary occupation probability of node i actually depends both on the value of the property x_i of node i and on the value of x_j for all the neighbors j of i . In other words, p_i^* is affected by the presence of degree-degree correlations.

The motion rule of the biased random walk used in this work is a special case of (Eq. A1). In particular, the walk takes places on the energy transport layer (defined by the adjacency matrix $E = \{e_{ij}\}$) and the bias function is the α -power of the degree $k_j = \sum_\ell a_{j\ell}$ of the destination node in the synchronization layer (defined by the adjacency matrix $A = \{a_{ij}\}$), i.e.,

$$f_j = k_j^\alpha. \quad (\text{A5})$$

By plugging Eq. (A5) into Eq. (A4) we obtain the expression for the stationary occupation probability

$$p_i^* = \frac{k_i^\alpha \sum_j e_{ij} k_j^\alpha}{\sum_\ell k_\ell^\alpha \sum_j e_{\ell j} k_j^\alpha}. \quad (\text{A6})$$

We note that Eq. (A6) depends on the degree-degree correlations that may exist in the synchronization layer. However, in this study we have focused on uncorrelated graphs, so that in practice the stationary distribution of walkers on a node i will depend, in a large enough network, primarily on the degree of node i on the synchronization layer.

Appendix B: Synchronization Theory

Here we present the full derivation of Eqs. (5) and (6) that provide an approximate description of the steady-state synchronization dynamics. In the following analysis, which closely follows and extends that described in Ref. [31], we will assume a sufficiently large network

and neglect any structural, e.g., degree-degree, correlations. Additionally, we will assume that no strong community structure exists in the network. We will search for synchronized solutions ($r > 0$) whose synchronized population has a constant angular velocity Ω . In many cases, particularly for strongly synchronized solutions, Ω can be reasonably approximated by the mean frequency $\Omega \approx \sum_i \omega_i / N$, however, in our analysis we will find a more accurate expression for Ω .

We begin by entering the rotating reference frame with (as of now, unspecified) angular velocity Ω by introducing the change of variables $\phi_i = \theta_i - \Omega t$. This transforms Eq. (3) into

$$\dot{\phi}_i = (\omega_i - \Omega) + \lambda \sum_{j=1}^N a_{ij} \sin(\phi_j - \phi_i). \quad (\text{B1})$$

We next introduce the set of local order parameters defined by

$$r_i e^{i\psi_i} = \sum_{j=1}^N a_{ij} e^{i\phi_j}, \quad (\text{B2})$$

whose magnitude r_i can be interpreted as a measure of synchronization among the network neighbors of node i . We note that precisely k_i terms contribute to r_i , as thus $r_i \in [0, k_i]$, as opposed to the global order parameter r , which is bounded by one. Using the definition of the local order parameters in Eq. (B2), Eq. (B1) simplifies to

$$\dot{\phi}_i = (\omega_i - \Omega) + \lambda r_i \sin(\psi_i - \phi_i). \quad (\text{B3})$$

Importantly, Eq. (B3) can be used to identify the dynamics of oscillator i given its ω_i , r_i , ψ_i , Ω , and λ . If $|\omega_i - \Omega| \leq \lambda r_i$, then Eq. (B3) has a stable fixed point that ϕ_i approaches. In particular, this fixed point is described by $\sin(\phi_i - \psi_i) = (\omega_i - \Omega) / \lambda r_i$. We refer to these oscillators as phase-locked, as by reaching this fixed point they join the synchronized population. On the other hand, if $|\omega_i - \Omega| > \lambda r_i$, then ϕ_i never reaches a fixed point and oscillator i drifts for all time. We refer to these oscillators as drifting.

To describe the global degree of synchronization of the system we will consider the family of local order parameters. To approximate each r_i we neglect the contribution due to drifting oscillators. While the drifting oscillators' contribution is not strictly zero due to the tendency for each drifting oscillator to spend more time near the minimum of $|\dot{\phi}_i|$ in Eq. (B3), We find that their contribution is second-order in comparison to that of the locked oscillators and neglect them for simplicity. Equation (B2) can then be rearranged and rewritten as

$$r_i = \sum_{|\omega_j - \Omega| \leq \lambda r_j} a_{ij} e^{i(\phi_j - \psi_i)}. \quad (\text{B4})$$

We now make two important simplifying assumptions. First, we assume that the average phases ψ_i and ψ_j of

each pair of network neighbors (i, j) is approximately equal, i.e., $\psi_i \approx \psi_j$. This is a reasonable assumption when the synchronized solution consists of a single synchronized cluster, as is typically the case when the network structure is not strongly modular. Second, we recall the definition of the local order parameters in Eq. (B2), noting that exactly k_i terms contribute to r_i . We propose that each r_i is proportional to its degree k_i , i.e., there exists some \tilde{r} such that $r_i \approx \tilde{r} k_i$ for all i . Both approximations are particularly accurate when the average nodal degree is not too small, thus improving the sampling of local averages. We note that these approximations have been used and verified in other synchronization literature [31–33]. It can be shown that the constant \tilde{r} is a good approximation for the global degree of synchronization r , and thus we will approximate $\tilde{r} \approx r$.

Under these assumptions, we expand the exponential in Eq. (B4) using cosine and sine and use that at steady-state phase-locked oscillators satisfy $\sin(\phi_i - \psi_i) = (\omega_i - \Omega) / \lambda r_i$ to obtain

$$r k_i = \sum_{|\omega_j - \Omega| \leq \lambda r k_j} a_{ij} \left[\sqrt{1 - \left(\frac{\omega_j - \Omega}{\lambda r k_j} \right)^2} + i \frac{\omega_j - \Omega}{\lambda r k_j} \right]. \quad (\text{B5})$$

Finally, we sum Eq. (B5) over all i , divide by N , and separate into real and imaginary parts to obtain, after some rearranging,

$$r = \frac{\langle k \rangle^{-1}}{N} \sum_{|\omega_j - \Omega| \leq \lambda r k_j} k_j \sqrt{1 - \left(\frac{\omega_j - \Omega}{\lambda r k_j} \right)^2}, \quad (\text{B6})$$

$$\Omega = \frac{\sum_{|\omega_j - \Omega| \leq \lambda r k_j} \omega_j}{\sum_{|\omega_j - \Omega| \leq \lambda r k_j} 1}. \quad (\text{B7})$$

Eqs. (B6) and (B7), which match Eqs. (5) and (6), jointly describe the steady-state synchronization dynamics given a sequence of degree-frequency pairs $\{(k_i, \omega_i)\}_{i=1}^N$ and can be solved self-consistently for r and Ω . In principle, the sums in Eqs. (B6) and (B7) can be transformed into integrals in the limit $N \rightarrow \infty$, however here we use the sums. We also note that, while $\{k_i\}_{i=1}^N$ is the degree sequence for the synchronization layer, the corresponding frequency sequence $\{\omega_i\}_{i=1}^N$ depends on both the degree sequence of the synchronization layer, as well as the structure of the energy layer. In particular, in our formulation we have that $\omega_i = N p_i^*$, where p_i^* is the stationary probability describing the fraction of random walkers at node i and is given by Eq. (A6).

Appendix C: Additional figures

We showed that spontaneous synchronization emerges for a wide range of the biasing parameter α . Here we show that spontaneous synchronization emerges for many different combinations of network structures as well. We

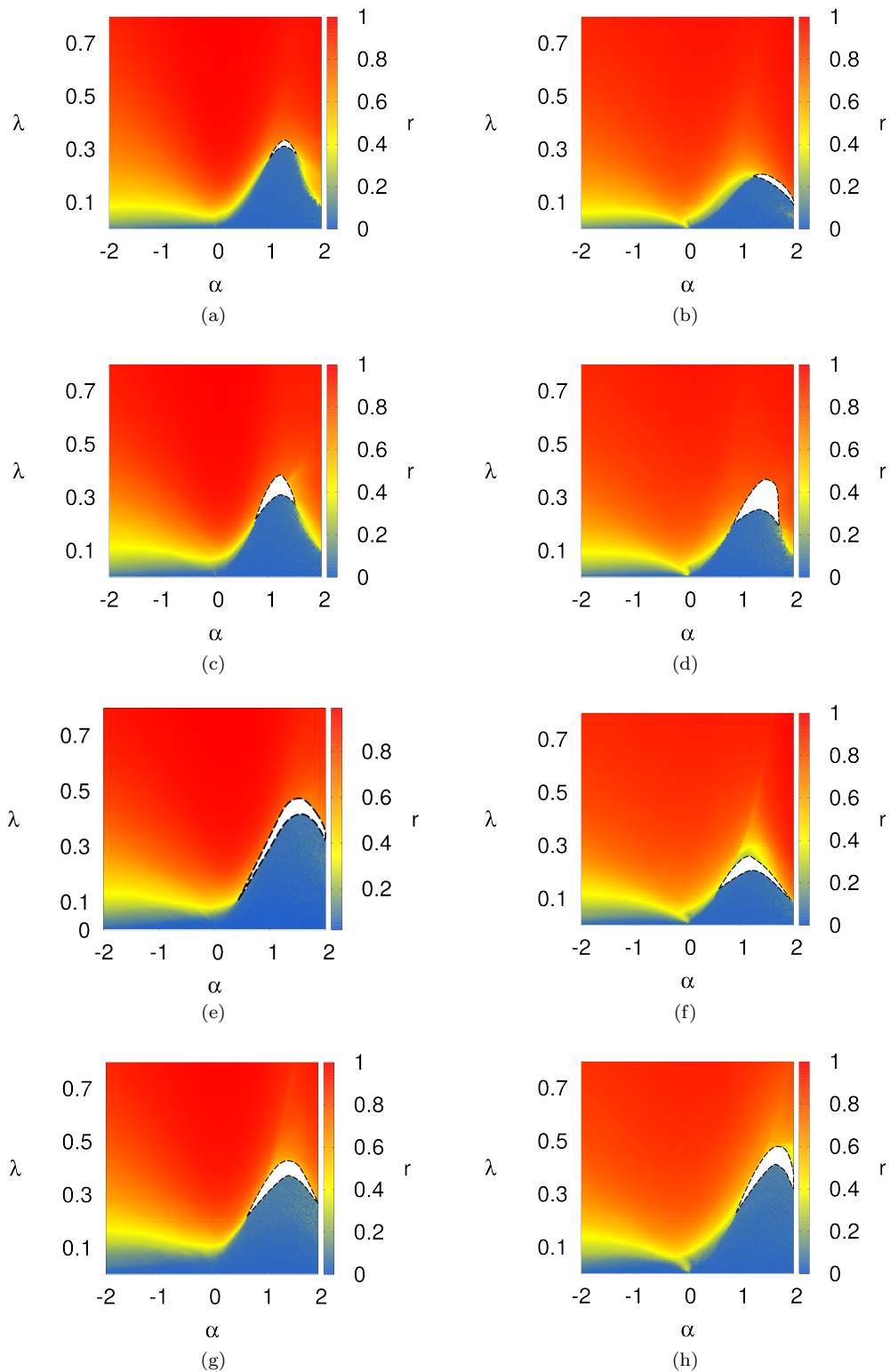


FIG. 4. Phase diagram of the system for different topologies of the energy transport layer (respectively, Erdős-Renyi on the left, scale-free configuration model random graphs with $P(k) \sim k^{-2.8}$ on the right) and of the synchronization layer (scale-free graphs with $P(k) \sim k^{-\gamma}$, with γ respectively equal to 2.2, 2.5, 2.8 and 3.0, from top to bottom). Independently of the actual combination of layer topologies, we always observe a relatively large interval of α in which the synchronization transition is abrupt.

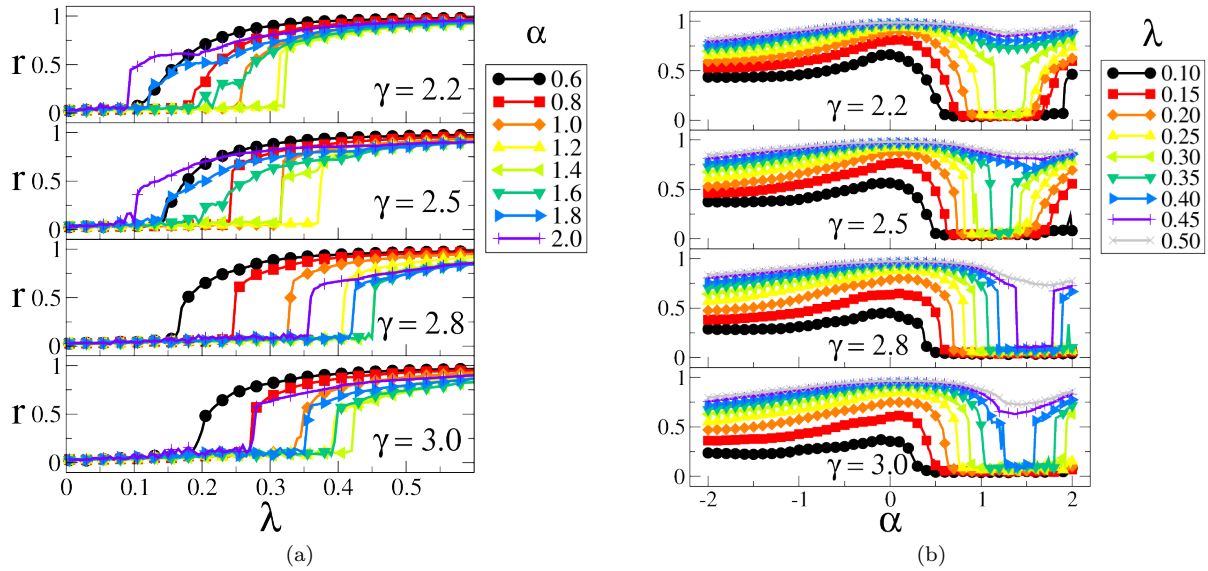


FIG. 5. (a) Forward synchronization diagrams corresponding to different values of the motion bias α and different exponents of the scale-free degree distribution on the synchronization layer (the energy transport layer is an Erdős-Rényi graph with $p = 0.01$). It is evident that the actual interval of α values in which we observe a sharp synchronization transition actually depends on the topology of the synchronization layer. (b) Cross-section of the phase diagrams reported in Fig. 4 (left) for different fixed values of λ as a function of α . Interestingly, it is possible to force the system either in a incoherent or synchronized state not only by tuning the coupling strength λ , but also the motion bias α . Notice that for some values of λ the transition to synchronization as a function of α is sharp.

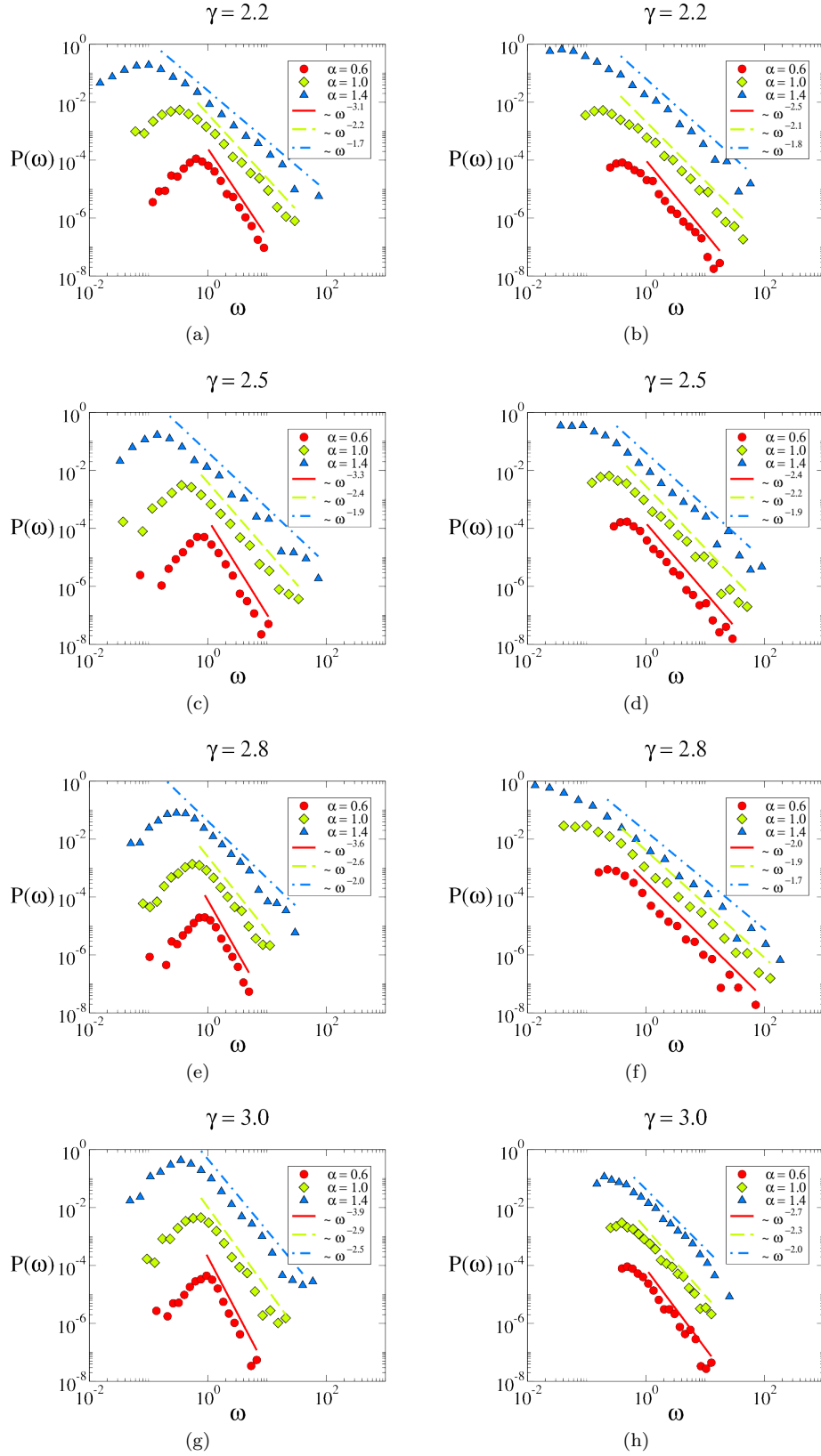


FIG. 6. The distribution of natural frequencies, as induced by the distribution of random walkers on an Erdős-Rényi (left) and a scale-free energy transport layer (right) for several values of α and different exponents of the degree distribution at the synchronization layer. The qualitative behavior of the distribution remains the same: it has a broad power-law-like tail independently of the topology of the two layers, and the major effect of different topologies is just a tuning of the exponent of this tail. Remarkably, higher values of α contribute to the broadening of the distribution $P(\omega)$.

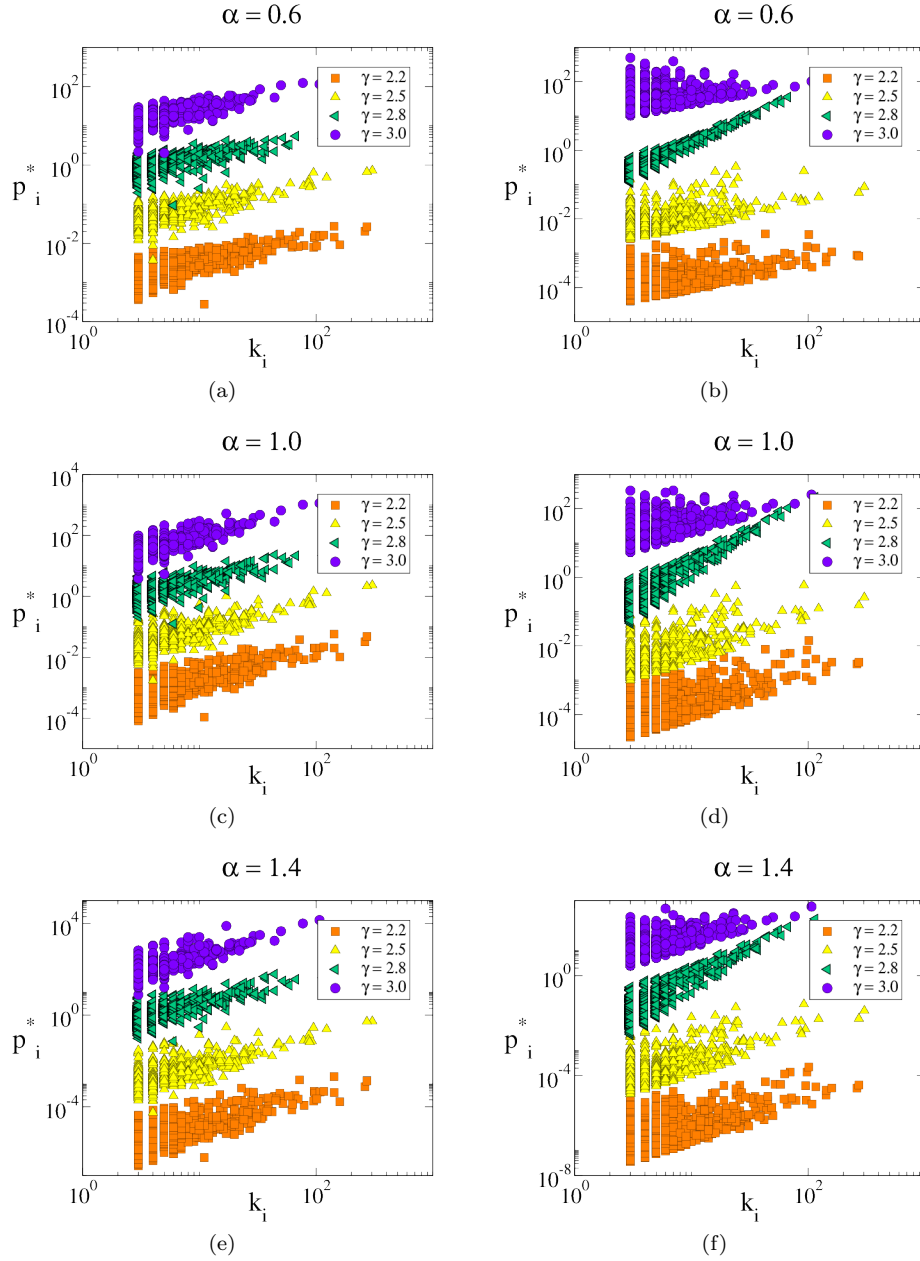


FIG. 7. Scaling of the stationary node occupation probability p^* for Erdős-Renyi (left) and scale-free (right) energy transport layers, different values of α and different values of the exponent γ of the degree distribution on the synchronization layer. The major visible effect of the heterogeneity of the synchronization layer on the scaling of p^* as a function of k is an attenuation of the fluctuations when γ increases.

report here additional plots of the phase diagram, synchronization profiles, frequency distribution, and scaling of the stationary energy distribution p_k^* for all the combinations of two different topologies of the energy transport layer, namely an Erdős-Rényi graph with connection probability $p = 0.01$ (ER) and a scale-free configuration model random graph with $P(k) \sim k^{-\gamma}$ for $\gamma = 2.8$ (SF-2.8) and four different topologies of the synchronization layer graph, namely scale-free configuration model random graphs with $P(k) \sim k^{-\gamma}$ for $\gamma = 2.2, 2.5, 2.8, 3.0$ (respectively denoted SF-2.2, SF-2.5, SF-2.8 and SF-3.0).

In Fig. 4 we show the phase diagrams in the $\alpha - \lambda$ plane, for ER (left) and SF-2.8 (right) energy transport layer and for increasing values of the exponent γ of the degree distribution of the synchronization layer. We note qualitatively equivalent behavior for all cases indicating that spontaneous synchronization is robust to all combinations of structure of the two layers. We always observe a sharp synchronization transition in an interval of positive values of α , usually between $\alpha \simeq 0.6$ and $\alpha \simeq 1.5$, even if the precise width of such interval depends on the topology of the two layers.

In Fig. 5 we compare some relevant cross-sections of these phase diagrams that correspond to the forward synchronization profiles for the ER transport layer for fixed (a) α and (b) λ . It is interesting to notice that, in addition to it being possible to control the degree of synchronization for fixed α by changing λ , for relatively wide ranges

of fixed λ it is possible to control the degree of synchronization by changing α . Furthermore, for both cases for the transition between incoherence and synchronization is often sharp.

In Fig. 6 we show the distribution of natural frequency for the eight combinations of layer topologies reported in Fig. 4. In general, the qualitative behavior of the system is preserved, so that higher values of the motion bias correspond to broader distributions of frequencies. The quantitative difference between the case of ER and SF-2.8 energy transport layer (different exponents of $P(\omega)$) is due to the difference in the expected average degree of the first neighbors of a node in an Erdős-Rényi graph and in an uncorrelated scale-free network, which concurs to determine the shape of the distribution of frequencies. In fact, in the former case the average degree of the first neighbors of a node scales as $\langle k \rangle$ (which is a constant), while in the latter one it scales as $\langle k^2 \rangle / \langle k \rangle$ and depends on the exponent of the degree distribution of the energy transport layer.

Finally, in Fig. 7 we present the scaling of p^* with k for different values of the motion bias α for ER (left) and SF-2.8 (right) transport layers. We notice again that the qualitative behavior of p_i^* does not heavily depend on the topology of the energy transport layer, while the exponent of the degree distribution of the synchronization layer actually affects the magnitude of the fluctuations around the expected scaling.

-
- [1] Newman, M. E. J. The structure and function of complex networks. *SIAM Review* **45**, 167–256 (2003).
- [2] Boccaletti, S., Latora, V., Moreno, Y., Chavez, M. & Hwang, D.-U. Complex networks: structure and dynamics. *Phys. Rep.* **424**, 175–308 (2006).
- [3] Strogatz, Steven H. Exploring complex networks. *Nature* **410**: 268–276 (2001).
- [4] Buldyrev, S.V., Parshani, R., Paul, G., Stanley, H.E. & Havlin, S. Catastrophic cascade of failures in interdependent networks. *Nature* **464**, 1025–1028 (2010).
- [5] Granell, C., Gomez, S. & Arenas, A. Dynamical interplay between awareness and epidemic spreading in multiplex networks. *Phys. Rev. Lett.* **111**, 128701 (2013).
- [6] Edvinsson, L. & Krause, D. N. Eds. *Cerebral Blood Flow and Metabolism, 2nd Edition* (Williams & Wilkins, Philadelphia, 2002).
- [7] Deco, G., Jirsa, V. K. & McIntosh, A. R. Resting brains never rest: computational insights into potential cognitive architectures. *Trends Neurosci.* **36**, 268–274 (2013).
- [8] Bullmore, E. & Sporns, O. Complex brain networks: graph theoretical analysis of structural and functional systems. *Nat. Rev. Neurosci.* **10**, 186–198 (2009).
- [9] Gao, J., Buldyrev, S. V., Stanley, H. E. & Havlin, S. Networks formed from interdependent networks. *Nature Phys.* **8**, 40–48 (2011).
- [10] Verbrugge, L. M. Multiplexity in adult friendships. *Social Forces* **57**, 1286–1309 (1979).
- [11] De Domenico, M. et al., *Phys. Rev. X* **3**, 041022 (2013).
- [12] Nicosia, V., Bianconi, G., Latora, V. & Barthelemy, M., *Phys. Rev. Lett.* **111**, 058701 (2013).
- [13] Battison, F., Nicosia, V. & Latora, V. Structural measures for multiplex networks, *Phys. Rev. E* **89**, 032804 (2014).
- [14] Gómez-Gardeñes, J. & Latora, V. Entropy rate of diffusion processes on complex networks. *Phys. Rev. E* **78**, 065102 (2008).
- [15] Kuramoto, Y. *Chemical Oscillations, Waves, and Turbulence* (Springer, New York, 1984).
- [16] Arenas, A., Díaz-Guilera, A., Kurths, J., Moreno, Y. & Zhou, C. Synchronization in complex networks. *Phys. Rep.* **469**, 93–153 (2008).
- [17] Malonek, D., Dirnagl, U., Lindauer, U., Yamada, K., Kanno, I. & Grinvald, A. Vascular imprints of neuronal activity: Relationships between the dynamics of cortical blood flow, oxygenation, and volume changes following sensory stimulation. *Proc. Natl. Acad. Sci. U.S.A.* **94**(26), 14826–14831 (1997).
- [18] Sheth, S. A., Nemoto, M., Guiou, M., Walker, M., Pouratian, N. & Toga, A. W. Linear and Nonlinear Relationships between Neuronal Activity, Oxygen Metabolism, and Hemodynamic Responses. *Neuron* **42**(2), 347–355 (2004).
- [19] Allen, E. A., Pasley, B. N., Duong, T. & Freeman, R.D. Transcranial magnetic stimulation elicits coupled neural and hemodynamic consequences. *Science* **317**(5846), 1918–1921 (2007).
- [20] Erdős, P. & Rényi, A. On the evolution of random graphs. *Pub. Math. Inst. Hung. Acad. Sci.* **5**, 17–61 (1960).

- [21] Bekessy, A., Bekessy, P. & Komlos, J. Asymptotic enumeration of regular matrices. *Stud. Sci. Math. Hung.* **7**, 343–353 (1972).
- [22] Gómez-Gardeñes, J., Gómez, S., Arenas, A. & Moreno, Y. Explosive synchronization transitions in scale-free networks. *Phys. Rev. Lett.* **106**, 128701 (2011).
- [23] Leyva, I., Sendiña-Nadal, I., Almendral, A., Buldú, J. M., Zanin, M., Papo, D. & Boccaletti, S. Explosive transitions to synchronization in networks of phase oscillators. *Sci. Rep.* **3**, 1281 (2013).
- [24] Zhang, X., Hu, X., Kurths, J. & Liu, Z. Explosive synchronization in a general complex network. *Phys. Rev. E.* **88**, 010802(R) (2013).
- [25] Iadecola, C. Neurogenic control of the cerebral microcirculation: is dopamine minding the store? *Nat. Neurosci.* **1**, 263–265 (1998).
- [26] Krimer, L. S., Muly, E. C., Williams, G. V. & Goldman-Rakic, P. S. Dopaminergic regulation of cerebral cortical microcirculation. *Nat. Neurosci.* **1**, 286–289 (1998).
- [27] Raichle, M. E. et al. A default mode of brain function. *Proc. Natl Acad. Sci. USA* **98**, 676–682 (2001).
- [28] Greicius, M. D., Krasnow, B., Reiss, A. L. & Menon, V. Functional connectivity in the resting brain: A network analysis of the default mode hypothesis. *Proc. Natl. Acad. Sci. U.S.A.* **100**(1), 253–258 (2002).
- [29] Goñi, J. et al. Resting-brain functional connectivity predicted by analytic measures of network communication. *Proc. Natl. Acad. Sci. USA* **111**(2), 833 (2013).
- [30] Honey, C. J., Kötter, R., Breakspear, M. & Sporns, O. Network structure of cerebral cortex shapes functional connectivity on multiple time scales. *Proc. Natl. Acad. Sci. USA* **104**(24), 10240–10245 (2007).
- [31] P. S. Skardal, J. Sun, D. Taylor, and J. G. Restrepo, *Europhys. Lett.* **101**, 20001 (2013).
- [32] T. Ichinomiya, *Phys. Rev. E* **70**, 026116 (2004).
- [33] J. G. Restrepo, E. Ott, and B. R. Hunt, *Phys. Rev. E* **71**, 036151 (2005).